Theoretical treatment of double photoionization of helium using a B-spline implementation of exterior complex scaling

C. William McCurdy,[1,2,3,*] Daniel A. Horner,[1,3,†] Thomas N. Rescigno,[1,‡] and Fernando Martín[4,§]

[1] *Lawrence Berkeley National Laboratory, Computing Sciences, Berkeley, California 94720*
[2] *Department of Applied Science, University of California, Davis, California 95616*
[3] *Department of Chemistry, University of California, Berkeley, California 94720*
[4] *Departamento de Química C-9, Universidad Autónoma de Madrid, 28049 Madrid, Spain.*

Calculations of absolute triple differential and single differential cross sections for helium double photoionization are performed using an implementation of exterior complex scaling in B-splines. Results for cross sections, well-converged in partial waves, are presented and compared with both experiment and earlier theoretical calculations. These calculations establish the practicality and effectiveness of the complex B-spline approach to calculations of double ionization of atomic and molecular systems.

PACS numbers: 32.80.Fb,34.10.+x

I. INTRODUCTION

The problem of double photoionization of helium is of fundamental interest because it provides the model for much of the basic physics for double photoionization of atoms and molecules in general. For that reason it has been the subject of extensive study by experimental [1–7] and theoretical methods.

For theoretical calculations the challenge is to correctly treat the boundary conditions for the breakup of a system of three charged particles. That problem has been recognized as both a formal and practical difficulty since the 1960s [8–10] and has been treated by a number of methods over the last decade with varying degrees of formal rigor and numerical accuracy. For example, an ansatz wave function with an explicit three-body asymptotic form was used in the three Coulomb wave (3C) approach [11–13], while Shakeshaft and coworkers made use of an assumed final state of screened Coulomb waves [14, 15] in a similar ansatz approach. The first numerical solutions of the Schrödinger equation for this problem were perfomed using the convergent close coupling [16–19] approach in which two-body boundary conditions are used in close-coupling calculations and three-body breakup amplitudes are constructed from two-body discrete channel amplitudes. More recently Selles *et al.* [20] developed a method in which semiclassical outgoing waves were combined with the hyperspherical R-matrix method to impose outgoing three-body boundary conditions in calculations of considerable accuracy. Another successful approach is the time-dependent close coupling method which applies the correct boundary conditions implicitly by time propagation of the initial state [21, 22] in a method that produces accurate results for this and other Coulomb breakup problems. Finally, in a development related in both spirit and formalism to the one discussed here, the need to explicitly impose three-body asymptotic boundary conditions was circumvented using complex Sturmian basis functions in a mathematically elegant method developed by Pont and Shakeshaft [23].

A recent and particularly successful approach to the problem of imposing the correct three-body breakup boundary conditions is the method of exterior complex scaling (ECS) which has now been applied to a range of problems, and has provided a formally and practically complete solution for the three-body Coulomb breakup problem. The ECS approach has been implemented using finite elements [24, 25], finite difference [26], and with a combination of finite elements and the discrete variable representation (DVR) [27, 28]. It has produced essentially exact results for electron-impact ionization of hydrogen [29, 30], and has been implemented with pseudospectral methods [31, 32] to treat multiphoton detachment in the context of Floquet theory for atoms in intense fields. ECS has also been applied directly to wave packet propagation in the time-dependent Schrödinger equation with external fields [33].

In this paper we explore this problem with a recently developed implementation in B-splines [34]. The B-spline method has been applied to atomic [35, 36] and molecular [37, 38] photoionization problems and there now exists a well developed technology for such calculations [39–41]. An important property of B-splines is that they are able to span a large volume to any degree of accuracy without encountering the numerical problems that prevent the use of exponentially decreasing basis functions. This is crucial for the description of continuum states, especially when the asymptotic region is needed. In addition, B-spline basis sets are effectively complete, which is an ideal property in those problems where the entire spectrum is needed [39]. The double ionization continuum lies in this cathegory.

Our goal is to compare the ECS-B-spline approach to the problem of double photoionization with experiment

* cwmccurdy@lbl.gov
† dahorner@lbl.gov
‡ tnrescigno@lbl.gov
§ fernando.martin@uam.es

and the results of other theoretical methods, to establish its accuracy and effectiveness. The results in the present study lay the groundwork for the application of the ECS B-spline method to double photoionization of molecules.

II. THE IMPLEMENTATION OF EXTERIOR COMPLEX SCALING USING B-SPLINES

The details of this implementation have been discussed at length elsewhere [34], but we will provide a brief summary of the essential points here.

The ECS transformation that underlies this approach scales the coordinates only outside a fixed radius,

$$r \to \begin{cases} r & r \le R_0 \\ R_0 + (r - R_0)e^{i\eta} & r > R_0 \end{cases} \quad (1)$$

where R_0 defines the radius within which the wave function will be the usual function of real-valued coordinates, and η is a scaling angle. In an exact or converged calculation the solutions of the Schrödinger equation for $r < R_0$ do not depend on η. However as has been discussed elsewhere [28, 29, 42] setting $\eta \neq 0$ effectively imposes outgoing scattering boundary conditions on the two-electron final state of our problem. B-splines that scale according to this ECS transformation are defined by setting a series of knots $t_i \le t_{i+1}$ on the complex contour and by using the usual recursion relation [43] for B-splines of order k,

$$B_i^k(r) = \frac{r - t_i}{t_{i+k-1} - t_i} B_i^{k-1}(r) + \frac{t_{i+k} - r}{t_{i+k} - t_{i+1}} B_{i+1}^{k-1}(r) \quad (2)$$

together with the definition of B-splines of order $k = 1$

$$B_i^1(r) = \begin{cases} 1 & \text{for } t_i \le r < t_{i+1} \\ 0 & \text{otherwise} \end{cases} \quad (3)$$

A basis of B-splines is defined by a grid of breakpoints, ξ_i, coinciding with the knots, t_i (which may be multiple), that appear in the recursion relation above. The breakpoints can be placed arbitrarily on this contour but one of them and its corresponding knot must be placed at $t_i = R_0$. In this way, B_i^k has a discontinuous first derivative with respect to r at $r = R_0$, because the derivative of the contour itself is discontinuous at that point. The discontinuity in the first derivative of all the B-splines that span the point R_0 is essential to reproduce that of the exact wave function. Figure 1 shows a typical B-spline basis of order $k = 8$ and the discontinuities of the first derivatives at $r = R_0$. Only B-splines that straddle the point R_0 have both real and imaginary components. All other B-splines are real, whether they are on the complex part of the contour or not.

With the above definitions, all one- electron matrix elements are reduced to sums of complex integrals between breakpoints. In each interval, the integrals are performed using a Gauss- Legendre quadrature. Only

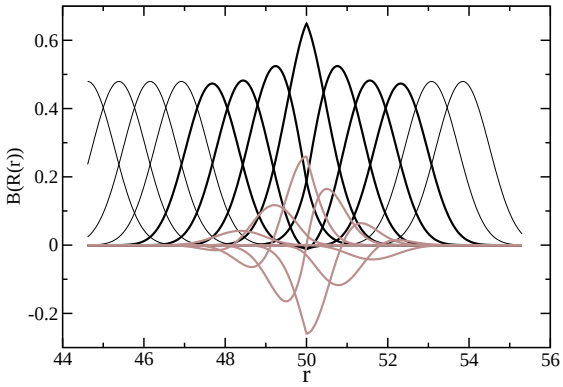

FIG. 1: 8th order B-splines on the complex exterior scaling contour with $R_0 = 50$ and $\eta = 40^0$. Heavy black lines are the real parts of the only complex splines. Grey lines are the imaginary parts.

those integrals involving B-splines that are both different from zero need to be evaluated. The two-electron integrals are performed by carrying out a multipole expansion of interelectron repulsion, $1/|\mathbf{r}_1 - \mathbf{r}_2|$. The angular portions of the two-electron matrix elements are evaluated analytically, while the radial portions are best handled by mapping the problem to an equivalent one involving the solution of Poisson's equation in an exterior complex-scaled B-spline basis. We refer the interested reader to ref. [34] for details.

III. THE AMPLITUDE AND CROSS SECTIONS FOR SINGLE PHOTON DOUBLE IONIZATION OF AN ATOM

The double photoionization amplitude is associated with the purely outgoing wave function Ψ_{sc}^+ that is the solution of the driven Schrödinger equation, which we can write for example in the "velocity form",

$$\begin{aligned} (E_0 + \omega - H)|\Psi_{sc}^+\rangle &= \epsilon \cdot (\nabla_1 + \nabla_2)\,|\Psi_0\rangle \\ &= \left(\frac{d}{dz_1} + \frac{d}{dz_2}\right)|\Psi_0\rangle \end{aligned} \quad (4)$$

where ϵ is the polarization unit vector, and $|\Psi_0\rangle$ is the initial (bound) state of the atom.

The asymptotic form of the solution of this equation can be written in analogy with Rudge's formal analysis of the electron-impact ionization problem [10],

$$\Psi_{sc}^+ \to -i^{1/2} \left(\frac{K^3}{\rho^5}\right)^{1/2} F(\hat{r}_1, \hat{r}_2, \alpha) e^{iK\rho + i\frac{\zeta}{K}\ln(2K\rho)} \quad (5)$$

where F is proportional to the ionization amplitude, the hyperradius, hyperangle and magnitude of the total mo-

mentum are

$$\begin{aligned} \rho &= \sqrt{r_1^2 + r_2^2} \\ \alpha &= \tan^{-1}(r_2/r_1) \\ K &= \sqrt{k_1^2 + k_2^2} \end{aligned} \tag{6}$$

and where the angle dependent coefficient of the logarithmic phase is

$$\zeta(\hat{r}_1, \hat{r}_2, \alpha)/\rho = 2/r_1 + 2/r_2 - 1/r_{12} \tag{7}$$

With the ECS method, the most effective approach for problems with two particles in the continuum is to write the amplitude as a surface integral performed on a surface just within the volume enclosed by the exterior scaling radius, R_0 [28, 44]. To that end we want to formulate the amplitude for this process as an integral of the form

$$f(\mathbf{k}_1,\mathbf{k}_2) = \left\langle \Phi^{(-)}_{Z_1}(\mathbf{k}_1, \mathbf{r}_1)\Phi^{(-)}_{Z_2}(\mathbf{k}_2, \mathbf{r}_2)|E - T - V_1|\Psi^+_{sc}\right\rangle \tag{8}$$

where E is the total energy, T is the two-electron kinetic energy operator, V_1 is the sum of all one-electron potentials,

$$V_1 = -Z_1/r_1 - Z_2/r_2 \tag{9}$$

The $\Phi^{(-)}_{Z_i}(\mathbf{k}, \mathbf{r})$ are Coulomb functions normalized to a delta function in momentum and with effective charges Z_i that will be defined later.

To relate the integral in Eq.(8) to the amplitude F, we can proceed to do the integral by stationary phase exactly as in Rudge's analysis [10]. His Eq. 2.52 is the result we seek, except for an overall factor of $(2\pi)^3$, which arises because our Coulomb functions are momentum normalized, and with a volume dependent overall phase which arises because we have not enforced the so-called "Peterkop condition" [8] on their effective charges.

So with Rudge's Eq. 2.52 we have

$$F(\mathbf{k}_1, \mathbf{k}_2, \beta) = -(2\pi)^{1/2}\chi(\mathbf{k}_1, \mathbf{k}_2, \rho)f(\mathbf{k}_1, \mathbf{k}_2) \tag{10}$$

with $\chi(\mathbf{k}_1, \mathbf{k}_2, \rho)$, being the usual (and irrelevant) volume dependent overall phase:

$$\begin{aligned} \chi(\mathbf{k}_1, \mathbf{k}_2, \rho) =& e^{-2iZ_2\ln(k_2/K)/k_2}e^{-2iZ_1\ln(k_1/K)/k_1} \\ & e^{i\left[\zeta(\hat{k}_1,\hat{k}_2,\beta)/K - Z_1/k_1 - Z_2/k_2\right]\ln(2K\rho)} \end{aligned} \tag{11}$$

The ζ function is, as defined by Rudge,

$$\zeta(\hat{k}_1, \hat{k}_2, \beta)/K = \frac{1}{k_1} + \frac{1}{k_2} - \frac{1}{|\mathbf{k}_1 - \mathbf{k}_2|} \tag{12}$$

and the hyperangle β, defined by $\beta = \tan^{-1}(k_2/k_1)$, parametrizes the asymptotic momentum distribution of the photoejected electrons. The original idea of the "Peterkop condition" was to make this overall volume-dependent phase disappear by choosing Z_1 and Z_2 to satisfy

$$\frac{Z_1}{k_1} + \frac{Z_2}{k_2} = \frac{1}{k_1} + \frac{1}{k_2} - \frac{1}{|\mathbf{k}_1 - \mathbf{k}_2|}, \tag{13}$$

which cancels the last exponent in Eq. (11). However the cross section for double photoionization does not depend in any way on this overall phase [45].

The triple differential cross section (TDCS) for double photoionization is directly related to the amplitude $f(\mathbf{k}_1, \mathbf{k}_2)$ by:

$$\frac{d^3\sigma}{dE_1 d\Omega_1 d\Omega_2} = \frac{4\pi^2}{\omega c}k_1 k_2 \left|f(\mathbf{k}_1, \mathbf{k}_2)\right|^2 \tag{14}$$

This result is the same as the one employed by Shakeshaft and coworkers [14, 15]. It is also consistent with the flux formulation of the problem of Selles *et al.* [20] who define the TDCS in terms of the outgoing flux associated with the solution of Eq.(4):

$$\begin{aligned} \frac{d^3\sigma}{dE_1 d\Omega_1 d\Omega_2} &= \tfrac{2\pi}{c\omega}\tfrac{\sin(2\alpha)}{4E}\rho^5 \lim_{\rho\to\infty} F_\rho(\Psi^+_{sc}) && (15) \\ &= \tfrac{2\pi}{\omega c}k_1 k_2 \left|F(\mathbf{k}_1, \mathbf{k}_2, \alpha)\right|^2 && (16) \end{aligned}$$

where $k_1 = K\cos(\alpha)$ and $k_2 = K\sin(\alpha)$ are the momenta of the outgoing electrons and the radial flux, F_ρ, is defined by

$$F_\rho(\Psi^+_{sc}) = \frac{1}{2i}\left(\Psi^{+*}_{sc}\frac{\partial}{\partial\rho}\Psi^+_{sc} - \Psi^+_{sc}\frac{\partial}{\partial\rho}\Psi^{+*}_{sc}\right) \tag{17}$$

Given the analysis of McCurdy, Horner and Rescigno [28], and the more complete analysis for electron impact ionization of hydrogen by Baertschy *et al.* [30], we know that we can evaluate the amplitude $f(\mathbf{k}_1, \mathbf{k}_2)$ by calculating the integral of eq. (8) on a finite volume, given the solution for Ψ^+_{sc} from an ECS B-spline calculation, *if we chose the effective charges to both be equal to the nuclear charge.*

$$Z_1 = Z_2 = 2 \tag{18}$$

With that choice the orthogonality properties of the Coulomb functions eliminate the contributions from the discrete single ionization channels, as has been discussed previously [28, 44], allowing for the use of values of the exterior scaling radius, R_0 that are of the order of a few 10's of Bohr radii for this problem.

There is an overall volume-dependent phase associated with this integral that has no physical consequences for calculations of the cross sections for this process. Moreover it has been shown that if for some reason it were interesting to do so, it can be calculated by an extension of the analysis of Rescigno, Baertschy and McCurdy [45].

An important practical consequence of Eq. (8) is that using Green's theorem it can be transformed into a surface integral that is easier to compute and that depends

only on the asymptotic form of the scattered wave function. That fact was exploited by Pont and Shakeshaft [23] and has been used extensively in calculations on electron-impact ionization using exterior complex scaling [27, 28, 30, 44, 45]. We will make use of this important property of Eq. (8) in our derivation below of the working equations for the present calculations.

The next question we must answer in order to do a practical calculation is how to define the *partial wave amplitudes* corresponding to Eq. (8) and how to express the triple differential cross sections and single differential cross sections in terms of them. It is to that question that we now turn our attention.

IV. REPRESENTATION OF Ψ_{sc}

In a calculation using the ECS B-spline approach we make use of configuration interaction (CI) representation of Ψ^+_{sc} of the form

$$\Psi^+_{sc} = \sum_{n,m,l_1<l_2} C_{nl_1,ml_2} \Phi_{n,l_1,m,l_2} \tag{19}$$

where C_{nl_1,ml_2} are the CI coefficients. The B-spline calculation has configurations defined by (total angular momentum L with upper/lower sign corresponding to singlet/triplet spin coupling)

$$\begin{aligned}\Phi_{n,l_1,m,l_2} = \frac{1}{\sqrt{2}}\frac{1}{r_1 r_2}\Big(&\varphi_{n,l_1}(r_1)\varphi_{m,l_2}(r_2)\mathcal{Y}^{L,M}_{l_1,l_2}(\Omega_1,\Omega_2)\pm \\ &\varphi_{m,l_2}(r_1)\varphi_{n,l_1}(r_2)\mathcal{Y}^{L,M}_{l_2,l_1}(\Omega_1,\Omega_2)\Big) \\ &(\alpha(1)\beta(2)\mp\beta(1)\alpha(2))/\sqrt{2}\end{aligned} \tag{20}$$

where $r^{-1}\varphi_{n,l}(r)$ denotes a normalized radial "orbital" associated with the indices nl.

If the initial state is ^1S, and is therefore spherically symmetric, and the polizarization is linear, we can choose any axis to coincide with the polarization vector ϵ. If we choose that to be the z axis, then the final state must have the symmetry $^1P_0$, where $M = 0$ corresponds to the z axis, because the dipole operator, for example in the length representation, $\epsilon \cdot \mathbf{r}$, transforms with $Y_{1,0}(\hat{\mathbf{r}})$. So for the case of double ionization of the helium ground state we have $L = 1$ and $M = 0$ in Eq. (20).

Thus we have written the scattered wave function in the form

$$\begin{aligned}\Psi^+_{sc} = \sum_{l_1<l_2}\Big(&\psi^{dir}_{l_1,l_2}(r_1,r_2)\mathcal{Y}^{L,M}_{l_1,l_2}(\Omega_1,\Omega_2)\pm \\ &\psi^{exch}_{l_1,l_2}(r_1,r_2)\mathcal{Y}^{L,M}_{l_2,l_1}(\Omega_1,\Omega_2)\Big)\end{aligned} \tag{21}$$

As we will see below, it is useful to visualize the partial wave radial wave functions, $\psi_{l_1,l_2}(r_1,r_2)$, in this equation.

The coupled spherical harmonics are defined by

$$\begin{aligned}&\mathcal{Y}^{L,M}_{l_1,l_2}(\Omega_1,\Omega_2) = \\ &\sum_{m_1,m_2}(l_1 m_1 l_2 m_2|l_1 l_2 L M)\, Y_{l_1,m_1}(\Omega_1)Y_{l_2,m_2}(\Omega_2)\end{aligned} \tag{22}$$

using the notation of Edmonds [46] for the vector coupling coefficients. In terms of 3-j symbols these functions are

$$\begin{aligned}&\mathcal{Y}^{L,M}_{l_1,l_2}(\Omega_1,\Omega_2) = \\ &\sum_{m_1,m_2}(-1)^{l_2-l_1-M}(2L+1)^{1/2} \\ &\begin{pmatrix} l_1 & l_2 & L \\ m_1 & m_2 & -M\end{pmatrix} Y_{l_1,m_1}(\Omega_1)Y_{l_2,m_2}(\Omega_2)\end{aligned} \tag{23}$$

and we will use their properties in deriving the expressions for the TDCS below.

V. PARTIAL WAVE ANALYSIS OF THE DOUBLE IONIZATION AMPLITUDE

A. The ionization amplitude and the triple differential cross section

As mentioned above, it is most effective in applications of the ECS approach to computing breakup amplitudes to formulate the amplitudes as surface integrals taken over a volume just inside the exterior scaling radius R_0. To get those working equations we now need to explicitly evaluate the integral expression for the double ionization amplitude

$$\begin{aligned}&f(\mathbf{k}_1,\mathbf{k}_2) = \\ &\left\langle \Phi^{(-)}(\mathbf{k}_1,\mathbf{r}_1)\Phi^{(-)}(\mathbf{k}_2,\mathbf{r}_2)|E-T-V_1|\Psi^+_{sc}\right\rangle\end{aligned} \tag{24}$$

where $\Phi^{(-)}(\mathbf{k},\mathbf{r})$ denotes a Coulomb function with momentum normalization and nuclear charge $Z = 2$. That function is related to the one with outgoing boundary conditions by $\Phi^{(-)}(\mathbf{k},\mathbf{r}) = \left(\Phi^{(+)}(-\mathbf{k},\mathbf{r})\right)^*$, and its partial wave expansion is given by [47]

$$\Phi^{(-)}(\mathbf{k},\mathbf{r}) = \left(\frac{2}{\pi}\right)^{1/2}\sum_{l,m}\frac{i^l e^{-i\eta_l}}{kr}\phi^{(c)}_{kl}(r)Y_{lm}(\hat{\mathbf{r}})Y^*_{lm}(\hat{\mathbf{k}}) \tag{25}$$

where

$$\eta_l = \arg\Gamma(l+1-iZ/k) \tag{26}$$

and the asymptotic form of the radial Coulomb function that defines its normalization is

$$\phi^{(c)}_{kl}(r) \to \sin(kr + \frac{Z}{k}\ln 2kr - \frac{\pi l}{2} + \eta_l) \tag{27}$$

Now we can substitute Eq.(25) and Eq.(19) [using Eq. (20)] into Eq.(24) to get the working equation for the ionization amplitude, $f(\mathbf{k}_1,\mathbf{k}_2)$, in terms of direct and exchange partial-wave amplitudes:

$$f(\mathbf{k}_1,\mathbf{k}_2) = \sum_{l_1<l_2} i^{-(l_1+l_2)} \Big(e^{i\eta_{l_1}(k_1)+i\eta_{l_2}(k_2)} \mathcal{F}^{dir}_{l_1l_2k_1k_2} \mathcal{Y}^{L,M}_{l_1,l_2}(\hat{\mathbf{k}}_1,\hat{\mathbf{k}}_2) \pm e^{i\eta_{l_1}(k_2)+i\eta_{l_2}(k_1)} \mathcal{F}^{exch}_{l_1l_2k_1k_2} \mathcal{Y}^{L,M}_{l_2,l_1}(\hat{\mathbf{k}}_1,\hat{\mathbf{k}}_2) \Big) \tag{28}$$

The double ionization amplitude has two contributions, one from the direct part and one from the exchange part of each of the CI configurations in Eq.(20). Note that the l_i indices are reversed in the coupled spherical harmonic in the exchange contribution and that the k's and l's appear paired differently in the direct and exchange contributions. The algebra that leads up to Eq.(28) involves first doing the angular integrations, which pick out the contributions to the coupled spherical harmonics in Eq.(20). The vector coupling coefficients are used to recombine the resulting terms to give coupled spherical harmonics that are function of the angles of ejection corresponding to the two momenta, $\mathbf{k}_1$ and $\mathbf{k}_2$. The other phase factors come from the two expansions of the Coulomb functions using Eq.(25).

Defining the one-electron radial Hamiltonians as

$$h_i = -\frac{1}{2}\frac{d^2}{dr_i^2} + \frac{l(l+1)}{2r_i^2} - \frac{2}{r_i} \tag{29}$$

the partial wave amplitudes in Eq.(28) are then given by

$$\begin{aligned} \mathcal{F}^{dir}_{l_1l_2k_1k_2} &= \frac{2}{\pi}\frac{1}{k_1k_2}\frac{1}{\sqrt{2}}\sum_{n,m} C_{nl_1,ml_2} \\ &\left\langle \phi^{(c)}_{k_1l_1}\phi^{(c)}_{k_2l_2} | E-h_1-h_2 | \varphi_{n,l_1}\varphi_{m,l_2} \right\rangle \\ &= \frac{2}{\pi}\frac{1}{k_1k_2}\frac{1}{\sqrt{2}}\sum_{n,m} C_{nl_1,ml_2} \\ &\int dr_1dr_2 \phi^{(c)}_{k_1l_1}(r_1)\phi^{(c)}_{k_2l_2}(r_2) \\ &(E-h_1-h_2)\varphi_{n,l_1}(r_1)\varphi_{m,l_2}(r_2) \end{aligned} \tag{30}$$

and

$$\begin{aligned} \mathcal{F}^{exch}_{l_1l_2k_1k_2} &= \frac{2}{\pi}\frac{1}{k_1k_2}\frac{1}{\sqrt{2}}\sum_{n,m} C_{nl_1,ml_2} \\ &\left\langle \phi^{(c)}_{k_1l_2}\phi^{(c)}_{k_2l_1} | E-h_1-h_2 | \varphi_{m,l_2}\varphi_{n,l_1} \right\rangle \\ &= \frac{2}{\pi}\frac{1}{k_1k_2}\frac{1}{\sqrt{2}}\sum_{n,m} C_{nl_1,ml_2} \\ &\int dr_1dr_2 \phi^{(c)}_{k_1l_2}(r_1)\phi^{(c)}_{k_2l_1}(r_2) \\ &(E-h_1-h_2)\varphi_{m,l_2}(r_1)\varphi_{n,l_1}(r_2) \end{aligned} \tag{31}$$

The "two-potential" formulas of Eq.(30) and Eq.(31) also have an equivalent surface integral representation of the partial-wave amplitudes, which appears upon the application of Green's theorem. By using the hyperspherical coordinates defined in Eq. (6), we can write each of them as an integral over a "surface" with $\rho=\rho_0$, which defines the volume in r_1 and r_2 for the integration

$$\begin{aligned} &\left\langle \phi^{(c)}_{k_1l_1}\phi^{(c)}_{k_2l_2} | E-h_1-h_2 | \varphi_{n,l_1}\varphi_{m,l_2} \right\rangle = \\ &\frac{\rho_0}{2}\int_0^{\pi/2} \Big[\phi^{(c)}_{k_1l_1}(r_1)\phi^{(c)}_{k_2l_2}(r_2)\frac{\partial}{\partial\rho}\varphi_{n,l_1}(r_1)\varphi_{m,l_2}(r_2) \\ &-\varphi_{n,l_1}(r_1)\varphi_{m,l_2}(r_2)\frac{\partial}{\partial\rho}\phi^{(c)}_{k_1l_1}(r_1)\phi^{(c)}_{k_2l_2}(r_2) \Big]\Big|_{\rho=\rho_0} d\alpha \end{aligned} \tag{32}$$

and

$$\begin{aligned} &\left\langle \phi^{(c)}_{k_1l_2}\phi^{(c)}_{k_2l_1} | E-h_1-h_2 | \varphi_{m,l_2}\varphi_{n,l_1} \right\rangle = \\ &\frac{\rho_0}{2}\int_0^{\pi/2} \Big[\phi^{(c)}_{k_1l_2}(r_1)\phi^{(c)}_{k_2l_1}(r_2)\frac{\partial}{\partial\rho}\varphi_{m,l_2}(r_1)\varphi_{n,l_1}(r_2) \\ &-\varphi_{m,l_2}(r_1)\varphi_{n,l_1}(r_2)\frac{\partial}{\partial\rho}\phi^{(c)}_{k_1l_2}(r_1)\phi^{(c)}_{k_2l_1}(r_2) \Big]\Big|_{\rho=\rho_0} d\alpha \end{aligned} \tag{33}$$

This representation makes it obvious that Eq.(24) and Eq.(28) depend only on the asymptotic form of Ψ^+_{sc}. In a practical calculation we choose ρ_0 to be just inside (a few tenths of a Bohr radius) R_0. The working equations with which we will compute the double ionization amplitudes are thus Eqs.(32-33) together with Eq.(28). The TDCS is then given by Eq.(14)

B. The singly differential cross section

The coupled spherical harmonics in Eq.(28) are orthornormal. Since the singly differential cross section is the integral of the TDCS in Eq. (14) over Ω_1 and Ω_2, it simplifies because of the orthonormality of the coupled spherical harmonics. The result is that the singly differential cross section (SDCS) is simply

$$\frac{d\sigma}{dE_1} = \frac{4\pi^2}{\omega c}k_1k_2\sum_{l_1l_2}\left(\left|\mathcal{F}^{dir}_{l_1l_2k_1k_2}\right|^2 + \left|\mathcal{F}^{exch}_{l_1l_2k_1k_2}\right|^2 \right) \tag{34}$$

and the phase factors in Eq.(28) do not play a role in its computation.

The total cross section for double ionization is then

$$\sigma_{ion} = \int_0^E \frac{d\sigma}{dE_1}dE_1 \tag{35}$$

although the integral cross section is frequently defined as the integral over half this interval, which requires a definition of the singly differential cross section as

$$\frac{d\tilde{\sigma}}{dE_1} = 2\frac{d\sigma}{dE_1} \tag{36}$$

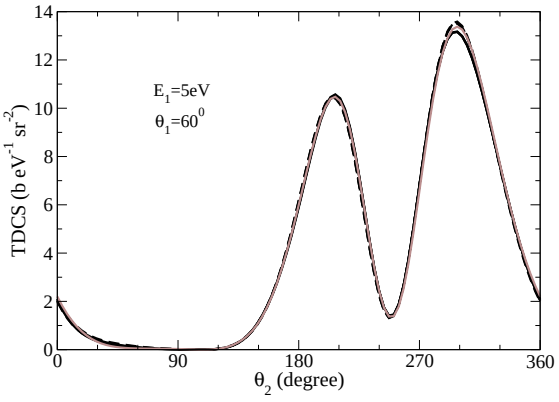

FIG. 2: TDCS for both length gauge (dashed curves) and velocity gauge (dark solid curves) for computational grids having $R_0 = 26\,a_0, 30\,a_0, 35\,a_0$. Light solid curve shows calculation including another double continuum, $l_1, l_2 = 4, 5$.

so that

$$\sigma_{ion} = \int_0^{E/2} \frac{d\tilde{\sigma}}{dE_1} dE_1 \tag{37}$$

Eq. (37) is, in fact, the convention used in this paper.

VI. CALCULATED CROSS SECTIONS FOR DOUBLE PHOTOIONIZATION OF HELIUM

The first requirement of accurate calculations of double photoionization cross sections is an accurate description of the ground state of the atom, because double ionization cross sections are largely determined by correlation effects in the initial state. For the ground state in these calculation we used configurations containing orbital angular momenta up to $l = 4$. The initial state is described by a CI wave function made up of Slater type orbitals with exponents of 2.4, 3.6, 4.8, 6.0 and 6.8 for $l = 0, ..., 4$ respectively, to give a total of 115 configurations. These Slater orbitals are expanded in the same B-spline basis described below. The ground state energy given by this calculation is -2.903198 hartree compared to the exact value [48] of -2.903724 hartree and is thus close to the $l = 4$ limit for the energy of the initial state.

For the final double continuum wave function, Ψ^+_{sc}, we have performed calculations with a variety of B-spline basis sets and included various numbers of partial waves for the double continuum. In Fig. 2 we show, as an example, the results of calculations in both the length and velocity gauges for the TDCS for a photon energy of 40 eV above the double ionization threshold. In that figure we include partial waves up to $l = 4$ and plot the results of calculations with values of the turning point R_0 for the ECS contour equal to $26\,a_0$, $30\,a_0$, and $35\,a_0$. We also show a calculation including up to $l = 5$ in the final state for $R_0 = 30\,a_0$. All calculations in Fig. 2 make use of 53 B-splines for each partial wave. The level of stability exhibited in Fig. 2 strongly suggests that these calculations are converged with respect to the computational parameters of the B-spline basis and partial wave expansion.

These calculations require much smaller values of R_0, and therefore smaller basis sets, than do calculations of electron impact ionization of hydrogen, for which a value of R_0 near $100\,a_0$ is necessary. We speculate that the reason for this behavior is that the final state of the double photoionization process in helium is more strongly dominated by the nuclear attraction potential. The fact that this interaction is included in the Coulomb functions of the "two-potential" integral expressions, Eqs.(32-33), with which we evaluate the amplitudes, allows them to be computed as a surface integral at values of the hyperradius corresponding to the point where that interaction begins to dominate the behavior of the outgoing wave.

All the results that we compare with experiment below were computed using a computational grid with 47 B-spline knot points over the first $42.0\,a_0$, and 6 additional knot points on the remaining complex contour out to $R_{\max} = 80\,a_0$. The turning point, R_0, of the ECS contour was $35.0\,a_0$. The angular momentum expansion included l values up to $l_{\max} = 4$, giving us contributions from the $kskp$, $kpkd$, $kdkf$, and $kfkg$ double continua. Using these 53 B-splines and 4 double continua, we have a total of 11,236 configurations in the CI representation of Ψ^+_{sc}. All the results we present below were computed in the velocity gauge, although as Fig. 2 indicates, the results in the length gauge are essentially the same.

The components of Ψ^+_{sc} defined in Eq.(21) reveal much of the dynamics of the photoionization process at a glance. The first three of them, the $kskp$, $kpkd$ and $kdkf$ contributions, are plotted in Fig. 3 for a photon energy 20 eV above the double ionization threshold. These plots show only the direct contribution and are thus not symmetric under interchange of r_1 and r_2. In the first of them we see the single ionization contribution as an outgoing wave parallel to the r_2 axis and confined to small r_1. The $kskp$ contribution also displays the outgoing waves for double ionization as wave fronts at constant hyperradius. For the higher angular components the relative importance of single ionization decreases since it proceeds through higher ionization thresholds; thus the outgoing double ionization wave fronts are more apparent. As l_1 and l_2 increase the wave function components rapidly decrease in magnitude as can be seen in the $kpkd$ contribution.

The SDCS for 20 eV is compared with experiment [1] and with the calculations of Colgan *et al.* [22] in Fig. 4. The agreement between these two calculations is very good. The partial wave contributions are also shown and demonstrate how the SDCS converges with inclusion of higher l values. The details of the TDCS, however, are naturally more sensitive to the higher angular momenta.

Braüning *et al.* [2] have measured absolute TDCS's for a photon energy of 20 eV above threshold. These

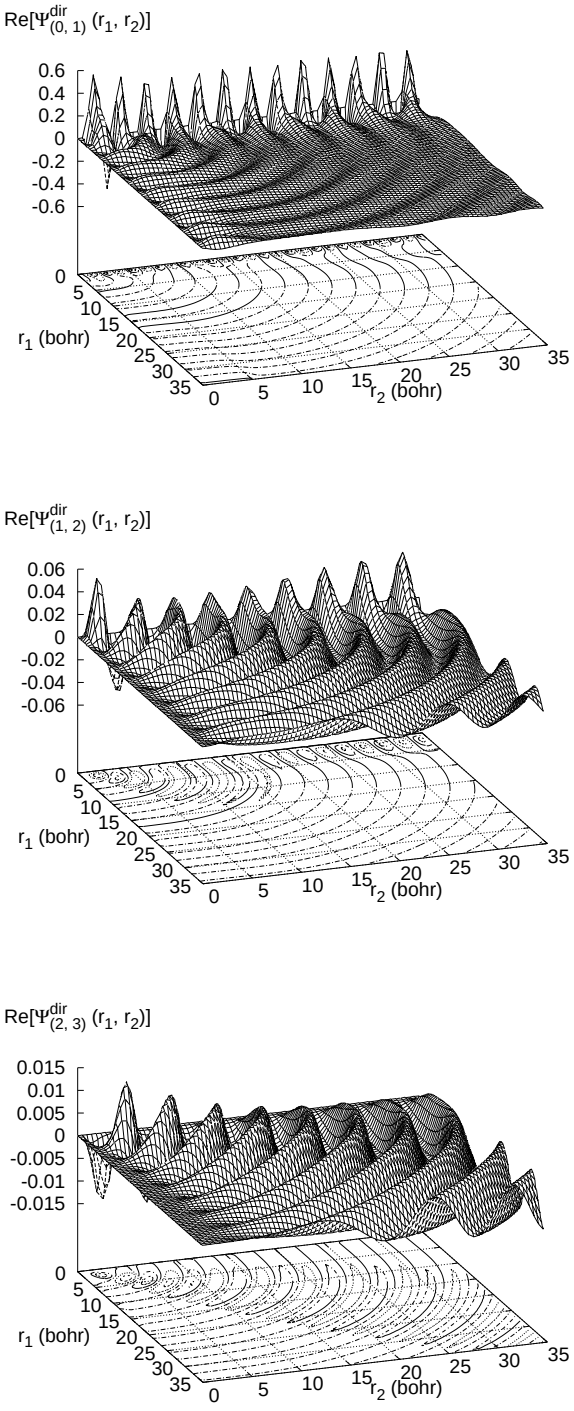

FIG. 3: Real part of of direct contribution to the wave function at 20 eV. The panels from top to bottom show the contributions from the *kskp*, *kpkd*, and *kdkf* partial waves.

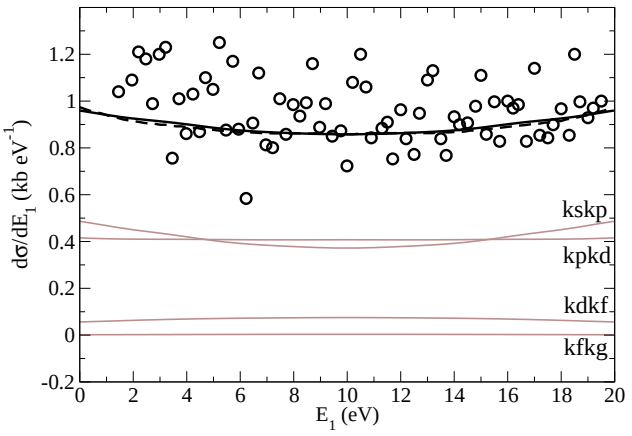

FIG. 4: SDCS for photon energy 20 eV above threshold. Circles: experiment by Wehlitz *et al.* [1]. Dashed curve: TD-CC calculations by Colgan *et al.* [22]. Thick solid curve: Present result. Lighter solid curves: contributions to SDCS from each noted double continuum.

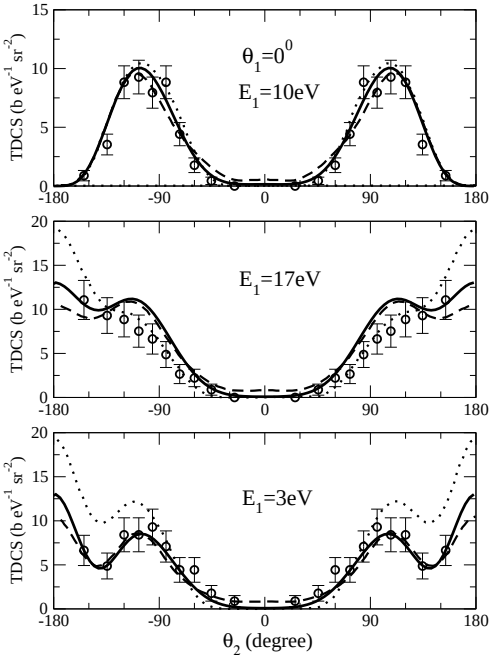

FIG. 5: TDCS for photon energy 20 eV above threshold, at various energy sharings for $\theta_1 = 0^0$. Circles: experiment by Braüning *et al.* [2]. Dashed curve: TD-CC calculations by Colgan *et al.* [22]. Dotted curve: HRM-SOW calculations by Selles *et al.* [20]. Thick solid curve: Present result.

measurements provide a rigorous test of the theoretical description of the double photoionization process and, thus, we begin by presenting results at this photon energy. Fig. 5 shows a comparison between our results and the experimental ones for $\theta_1 = 0^0$, i.e. for the case in which the first electron exits parallel to the polarization axis. The agreement is very good. The figure also

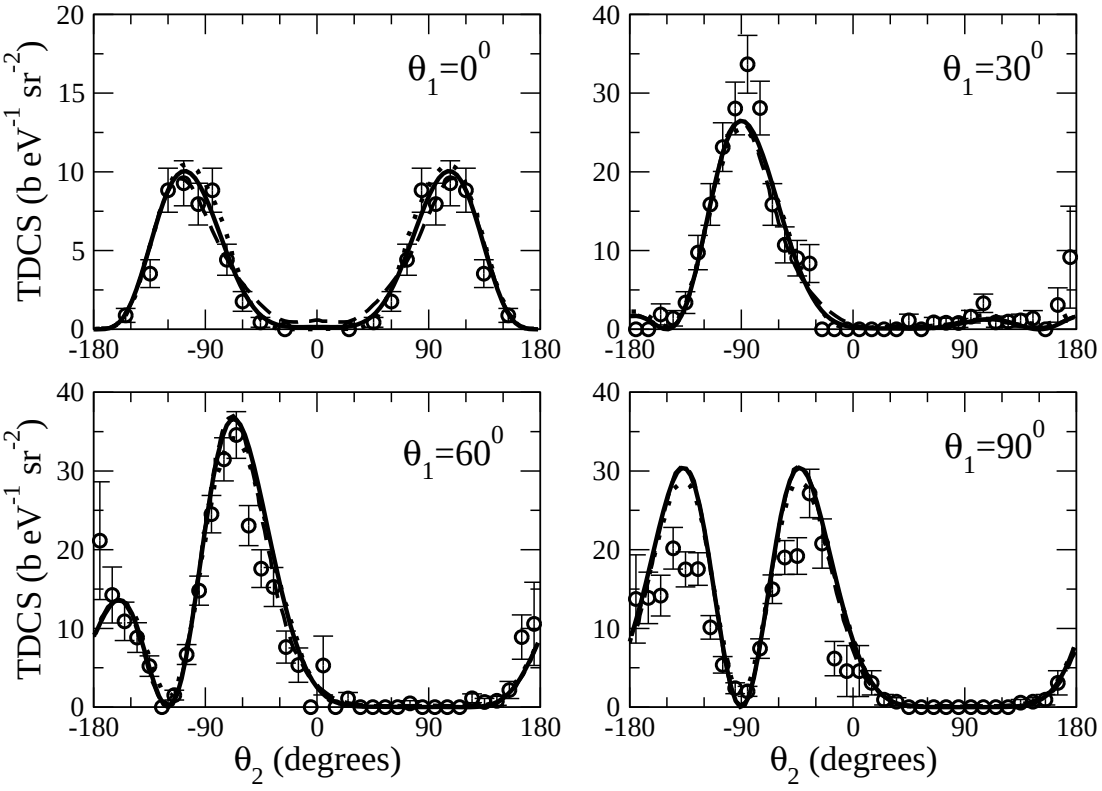

FIG. 6: TDCS for photon energy 20 eV above threshold, for various θ_1 values in equal energy sharing. Circles: experiment by Braüning *et al.* [2]. Dashed curve: TD-CC *et al.* [22]. Dotted curve: HRM-SOW [20]

includes results from previous theoretical calculations, namely results from the Time-Dependent Close-Coupling method of Colgan (TD-CC) *et al.* [22] and the Hyperspherical R-Matrix method with Semiclassical Outgoing Waves (HRM-SOW) method of Selles *et al.* [20]. Although the general agreement between different theoretical results is good, there are significant discrepancies when the two electrons escape "back-to-back" in directions colinear with the polarization vector. This geometry, which we might call the "Wannier geometry" because it is the geometry that dominates at threshold for electron-impact ionization, is the one that requires the most partial waves and densest basis to converge in the present calculations. Our results are closer to those of the TD-CC method.

For other geometries the agreement between various *ab initio* calculations is much better, and for them essentially identical results are obtained at 20 eV by ECS, TD-CC and HRM-SOW methods. As an illustration, Fig. 6 shows a comparison for equal energy sharing and different values of θ_1. A similar agreement between theoretical results from these three methods is found at all the other geometries reported here for 20 eV.

In Fig. 7 we compare the ECS results for unequal energy sharings with the absolute experimental determinations of Braüning *et al.* for $\theta_1 = 60^0$ and $\theta_1 = 90^0$. Fig. 8 shows a similar comparison for all the energy sharings measured by Braüning *et al.* at 20 eV and $\theta_1 = 30^0$. Very good agreement is obtained in all cases.

These experiments and essentially all others on this system were performed in "coplanar geometry", that is, with the polarization vector and both momenta $\mathbf{k}_1$ and $\mathbf{k}_2$ lying in the same plane. To provide an overall visualization of the double ionization process, we have also evaluated TDCS's for out-of-plane geometries. In Fig. 9 we show two three-dimensional views of the TDCS for a photon energy of 20 eV above threshold that correspond to two panels of Fig. 8. In the first one we see the effects on the three-dimensional TDCS of the selection rule for equal energy sharing that prevents the electrons from exiting in opposite directions [12]. The selection rule is more apparent in three dimensions than in Fig. 8. In the second case, for strongly unequal energy sharing ($E_1 = 3$ eV and $E_2 = 17$ eV), we see that the selection rule does not apply and a lobe appears in the TDCS corresponding to emission of the second electron in the opposite direction to the first, lower energy electron.

We now turn to the case of 40 eV for which the experiments of Bologonesi *et al.* [49] and those of Cvejanović *et al.* [50] provide only relative values of the cross sections. In each case the reported TDCS for different energy sharings and angles are internormalized within the experiment. So we have two separate sets of internormalized results with which to compare. Theoretical calculations

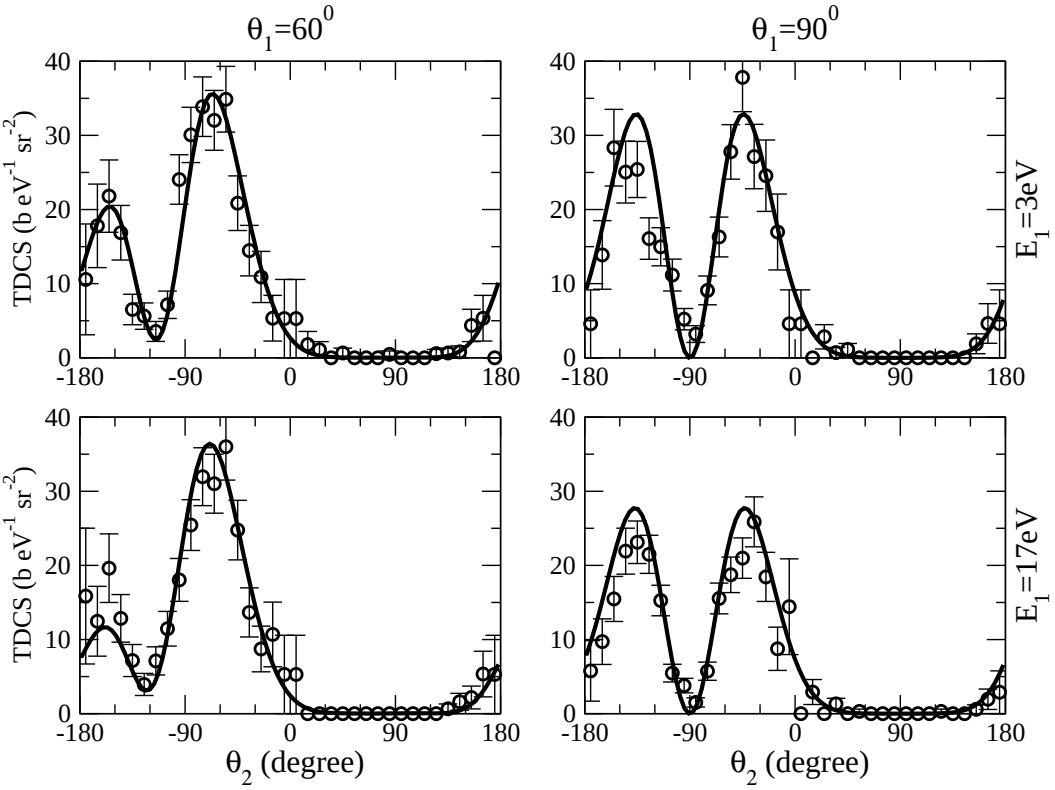

FIG. 7: TDCS for photon energy 20 eV above threshold, at energy sharings with $E_1 = 3$ eV (upper panels) and 17 eV (lower panels) for $\theta_1 = 60^0$ and $\theta_1 = 90^0$. Circles: experiment by Braüning *et al.* [2]. Thick solid curve: Present result.

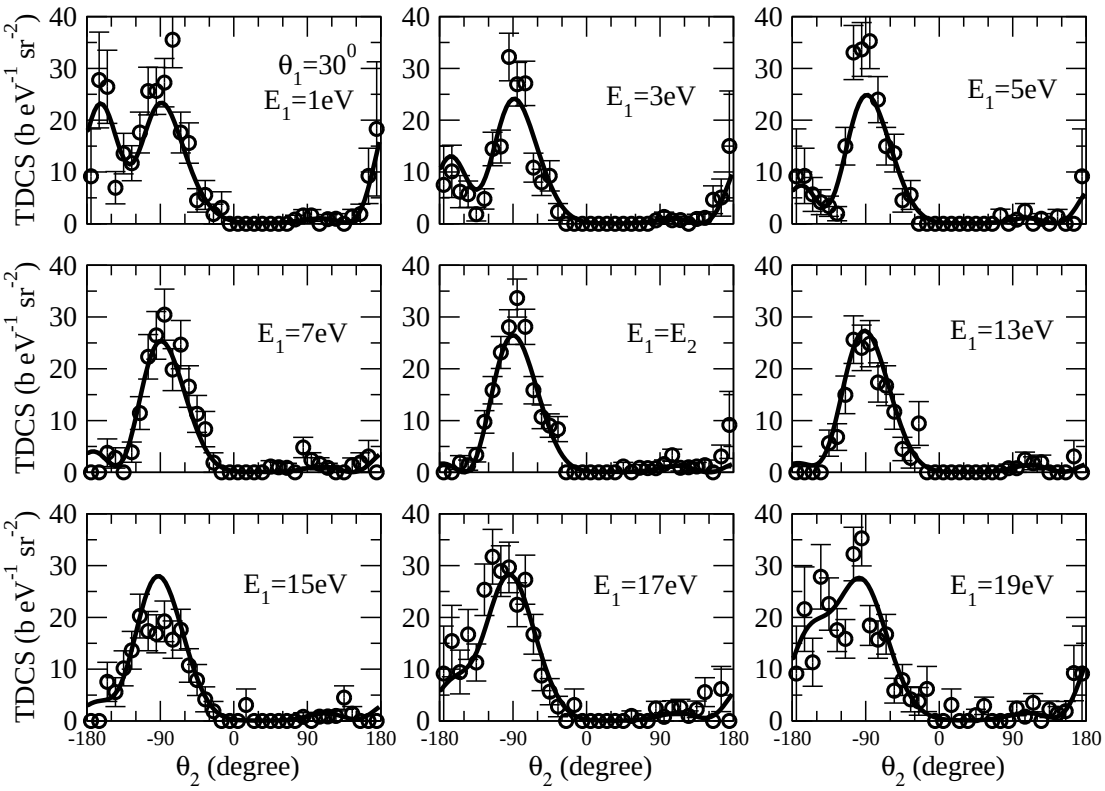

FIG. 8: TDCS at 20 eV above threshold for the geometry $\theta_1 = 30^0$, $\phi_1 = \phi_2$. The panels show various energy sharings with the energy E_1 given in each panel. Circles: experiment by Braüning *et al.* [2]. Solid curve: present results.

predict absolute values for cross sections. Therefore, we adhere here to the principle that no scaling of any theoretical TDCS predictions should be made when comparing them with experiment. To do otherwise would be misleading, especially when there are several theoretical predictions to be compared with the same experimental cross section.

In Fig. 10 we compare with the experimental results of Bolognesi *et al.* [49] and the results of CCC calculations included in the same reference for an energy sharing $E_1 = 5\,\text{eV}$ and $E_2 = 35\,\text{eV}$, and θ_1 varying from 0^0 to 60^0. We have normalized the relative experimental cross sections to our computed TDCS at $\theta_1 = 60^0$ and $\theta_2 = 30^0$ for this energy sharing, thereby fixing the normalization of the experiment in Fig. 10 as well as in Fig. 11 where we compare with complementary sets of experimental data for $E_1 = 35\,\text{eV}$ and $E_2 = 5\,\text{eV}$. The results of CCC calculations from reference [49] are also shown in those figures with no scaling. Although both theoretical results generally reproduce the shapes of these six TDCS plots, there remain significant differences between the theories and between the theories and the experiment. The CCC results are significantly smaller than the ECS results for $\theta_1 = 60^0$ and 30^0 in both figures. Nonetheless both theories suggest, as was originally suggested in reference [49], that the internormalization of the experiment for $E_1 = 5\,\text{eV}$ and $\theta_1 = 30^0$ and 0^0 may be suspect. The ECS results, however seem to be in better overall agreement with the results of this experiment.

Turning to the experiments of Cvejanović *et al.* [50] for a photon energy of 40 eV above threshold and $E_1 = 5\,\text{eV}$, we again normalize the relative cross sections to our computed TDCS value at one point, namely $\theta_1 = 130^0$ and $\theta_2 = 250^0$, thereby determining the normalization of all six TDCS plots in Figs. 12 and 13. In these figures we also plot the CCC results of reference [51]. Again, while the overall shapes of the cross sections are very similar and there is general quantitative agreement, some significant differences can be seen between the ECS and CCC computed results. Overall the CCC results seem to be in better agreement with this experiment, although both theoretical calculations differ from the experiment systematically. Those differences are particularly pronounced for the "Wannier geometry" where the electrons go out in opposite directions colinear with the polarization axis.

VII. CONCLUSION

We have evaluated triply differential cross sections (TDCS) for double photoionization of helium using a recent implementation of exterior complex scaling (ECS) with B-splines basis functions. This implementation

takes advantage of existing B-spline codes for atomic two-electron systems as well as of all the ECS technology developed to evaluate TDCS's in electron impact ionization problems. Details of the most important modifications in the current B-spline codes have been published elsewhere [34], while the link with the double photoionization problem has been presented in detail in this paper. The power of the ECS-B-spline approach resides in its ability to provide converged results to any desired accuracy without losing the possibility to work with atomic orbitals as in traditional basis sets expansions. This is a very important feature that allows one to reduce the size of the calculations without loosing accuracy and, therefore, it will be very convenient for future applications to more complicated systems such as diatomic molecules.

Application of this methodology to the evaluation of TDCS in double photoionization of helium has shown that converged results are obtained with a moderate number of basis functions and partial waves. Our results for a photon energy of 20 eV above threshold are in very good agreement with absolute measurements of Brauning *et al.* for all the coplanar geometries and energy sharings investigated here. There is also general good agreement with previous theoretical results obtained with the TDCC and HRM-SOW methods, although some discrepancies exist for unequal energy sharing when the two electrons escape in oposite directions. At this photon energy, we have also presented a few results for three-dimensional (non-coplanar) geometries for which previous experimental or theoretical results do not exist.

Similar conclusions have been obtained for a photon energy of 40 eV above threshold, although, in this case, the differences between the present results and those from a previous CCC calculation are significantly larger and these differences are not confined to geometries where the electrons escape in oposite directions.

Acknowledgments

This work was performed under the auspices of the US Department of Energy by the University of California Lawrence Berkeley National Laboratory under Contract DE-AC03-76SF00098 and was supported by the U.S. DOE Office of Basic Energy Sciences, Division of Chemical Sciences. The calculations were carried out at the National Energy Research Scientific Computing Center at Lawrence Berkeley National Laboratory. DAH acknowledges support from the U.S. DOE Computational Science Graduate Fellowship Program. The work of FM was supported by the *Dirección General de Investigación* (Spain), projects No. BFM2000-0033 and BQU2001-0147, and the European COST action D26/0002/02. CWM gratefully acknowldges a grant from the *Ministerio de Educación, Cultura y Deporte* (Spain) for a sabbatical research visit to the Universidad Autónoma de Madrid.

[1] R. Wehlitz, F. Heiser, O. Hemmers, B. Langer, A. Menzel, and U. Becker, Phys. Rev. Lett. **67**, 3764 (1991).
[2] M. Braüning, R. Dörner, C. L. Cocke, M. H. Prior, B. Kriässig, A. S. Kheifets, I. Bray, A. Braüning-Demian, K. Carnes, S. Dreuil, V. Mergel, P. Richard, J. Ulrich, H. Schmidt-Böcking, J. Phys. B **31**, 5149 (1998).
[3] V. Mergel, M. Achler, R. Dörner, K. Khayyat, T. Kambara, Y. Awaya, V. Zoran, B. Nyström, L. Spielberger, J. H. McGuire, J. Feagin, J. Berakdar, Y. Azuma, H. Schmidt-Böcking, Phys. Rev. Lett. **80**, 5301 (1989).
[4] J. A. R. Samson, W. C. Stolte, Z. X. He, J. N. Cutler, and Y. Lu, Phys. Rev. A **57**, 1906 (1998).
[5] J. P. Weightman, S. Cvejanović, and T. J. Reddish, J. Phys. B **31**, 1753 (1998).
[6] K. Soejima, A. Danjo, K. Okuno, and A. Yagishita, Phys. Rev. Lett. **83**, 1546 (1999).
[7] A. Huetz and J. Mazeau, Phys. Rev. Lett. **85**, 530 (2000).
[8] R. K. Peterkop, Opt. Spectrosc. **13**, 87 (1962).
[9] M. R. H. Rudge and M. J. Seaton, Proc. Roy. Phys. Soc. **283**, 262 (1965).
[10] M. R. H. Rudge, Rev. Mod. Phys. **40**, 564 (1968).
[11] M. Brauner, J. S. Briggs, and H. Klar, J. Phys. B **22**, 2265 (1989).
[12] F. Maulbetsch and J. S. Briggs, J. Phys. B **26**, 1679 (1993).
[13] J. Berakdar and J. S. Briggs, Phys. Rev. Lett. **72**, 3799 (1994).
[14] D. Proulx and R. Shakeshaft, Phys. Rev. A **48**, R875 (1993).
[15] M. Pont and R. Shakeshaft, Phys. Rev. A **51**, R2676 (1995).
[16] I. Bray and A. T. Stelbovics, Phys. Rev. A **46**, 6995 (1992).
[17] I. Bray and A. T. Stelbovics, Phys. Rev. A **54**, 2991 (1996).
[18] I. Bray, Phys. Rev. Lett. **78**, 4271 (1997).
[19] A. Kheifets and I. Bray, J. Phys. B **31**, L447 (1998).
[20] P. Selles, L. Malegat, and A. K. Kazansky, Phys. Rev. A **65**, 032711 (2002).
[21] F. Robicheaux, M. S. Pindzola, and D. R. Plante, Phys. Rev. A **55**, 3573 (1997).
[22] J.Colgan, M. S. Pindzola, and F. Robicheaux, J. Phys. B **34**, L457 (2001).
[23] M. Pont and R. Shakeshaft, Phys. Rev. A **51**, 494 (1995).
[24] C. W. McCurdy, T. N. Rescigno, and D. Byrum, Phys. Rev. A **56**, 1958 (1997).
[25] C. W. McCurdy and T. N. Rescigno, Phys. Rev. A **56**, R4369 (1997).
[26] M. Baertschy, T. N. Rescigno, W. A. Isaacs, and C. W. McCurdy, Phys. Rev. A **60**, R13 (1999).
[27] T. N. Rescigno and C. W. McCurdy, Phys. Rev. A **62**, 032706 (2000).
[28] C. W. McCurdy, D. A. Horner, and T. N. Rescigno, Phys. Rev. A **63**, 022711 (2001).
[29] T. N. Rescigno, M. Baertschy, W. A. Isaacs, and C. W. McCurdy, **286** (1999).

[30] M. Baertschy, T. N. Rescigno, and C. W. McCurdy, Phys. Rev. A **64**, 022702 (2001).
[31] D. A. Telnov and S.-I. Chu, Phys. Rev. A **66**, 043417 (2002).
[32] D. A. Telnov and S.-I. Chu, Phys. Rev. A **59**, 2864 (1999).
[33] C. W. McCurdy, C. K. Stroud, and M. K. Wisinski, Phys. Rev. A **43**, 5980 (1991).
[34] C. W. McCurdy and F. Martín, J. Phys. B **XX**, XXXX (2004).
[35] I. Sánchez, H. Bachau, and F. Martín, J. Phys. B **30**, 2417 (1997).
[36] A. Reber, F. Martín, H. Bachau, and R. S. Berry, Phys. Rev. A **65**, 0634131 (2002).
[37] I. Sánchez and F. Martín, Phys. Rev. Lett. **79**, 1654 (1997).
[38] I. Sánchez and F. Martín, Phys. Rev. Lett. **82**, 3775 (1999).
[39] H. Bachau, E. Cormier, P. Decleva, J. E. Hansen, and F. Martín, Reports on Progress in Physics **64**, 1815 (2001).
[40] F. Martín, J. Phys. B: At. Mol. Opt. Phys. **32**, R197 (1999).
[41] I. Sánchez and F. Martín, J. Phys. B **30**, 679 (1997).
[42] M. Baertschy, T. N. Rescigno, W. A. Isaacs, X. Li, and C. W. McCurdy, Phys. Rev. A **63**, 022712 (2001).
[43] C. de Boor, *A Practical Guide to Splines* (Springer, New York, 1978).
[44] C. W. McCurdy and T. N. Rescigno, Phys. Rev. A **62**, 032712 (2000).
[45] T. N. Rescigno, M. Baertschy, and C. W. McCurdy, Phys. Rev. A **68**, 020701 (2003).
[46] A. R. Edmonds, *Angular Momentum in Quantum Mechanics* (Princeton University Press, Princeton, 1957), p. 37ff.
[47] R. G. Newton, *Scattering Theory of Waves and Particles* (Springer-Verlag, New York, 1982), p. 424ff.
[48] G. W. F. Drake, M. M. Cassar, and R. A. Nistor, Phys. Rev. A **65**, 054501 (2002).
[49] P. Bolognesi, R. Camillion, M. Coreo, G. Turri, J. Berakdar, A. S. Kheifets, and L. Avaldi, J. Phys. B **34**, 3193 (2001).
[50] S. Cvejanović, J. Wingman, T. J. Reddish, F. Maulbetsch, M. A. MacDonald, A. S. Kheifets, and I. Bray, J. Phys. B **33**, 265 (2000).
[51] A. S. Kheifets and I. Bray, Phys. Rev. A **65**, 022708 (2002).

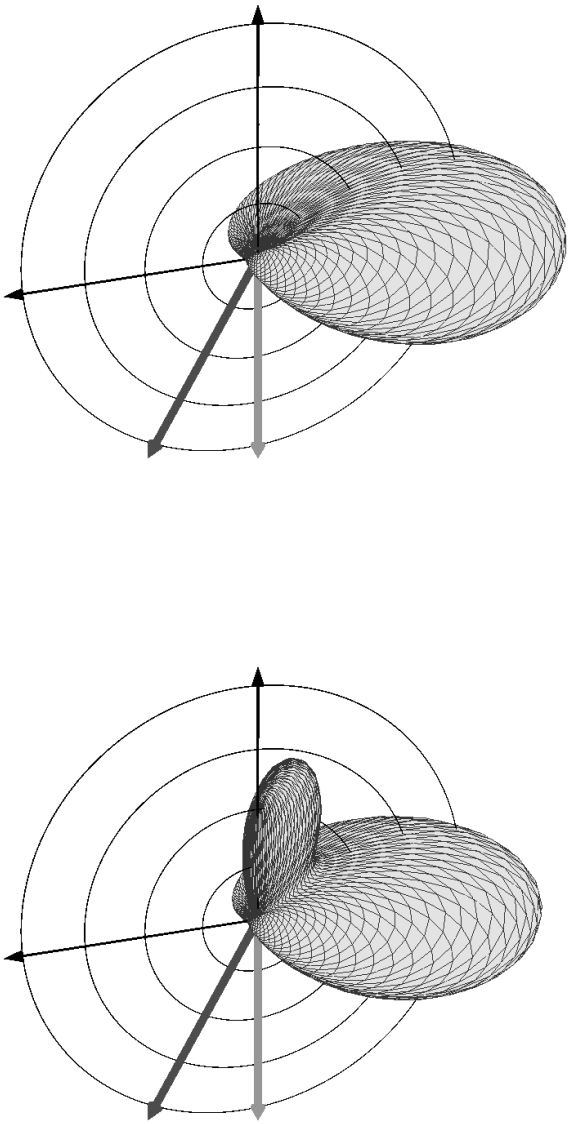

FIG. 9: Three dimensional TDCS plots for 20 eV. Lighter vertical arrrow pointing downward is the photon polarization direction to which all angles refer. Darker arrow represents the direction of one ejected electron, $\theta_1 = 30^0$. The surface shows the angular ejection distribution of the second electron, for the case of equal energy sharing, $E_1 = E_2 = 10$ eV (top panel), and unequal energy sharing, $E_1 = 3$ eV (bottom panel).

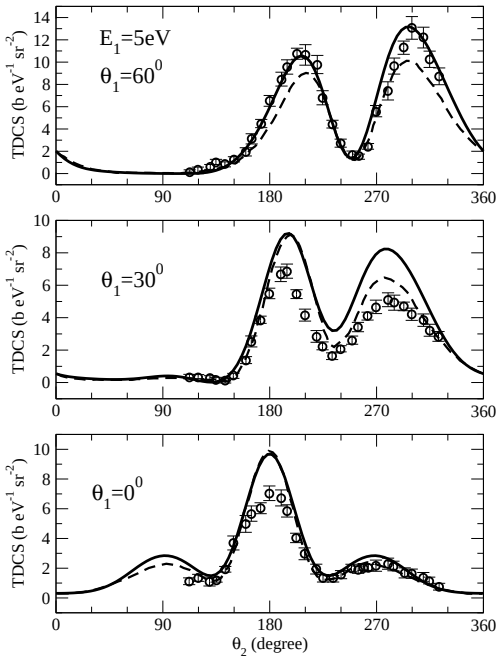

FIG. 10: TDCS for photon energy 40 eV above threshold, in the unequal energy sharing of $E_1 = 5$ eV and $E_2 = 35$ eV at various values of θ_1 of the 5 eV electron. Circles and dashed curve: experiment and CCC calculation of Ref. [49]. Thick solid curve: Present result.

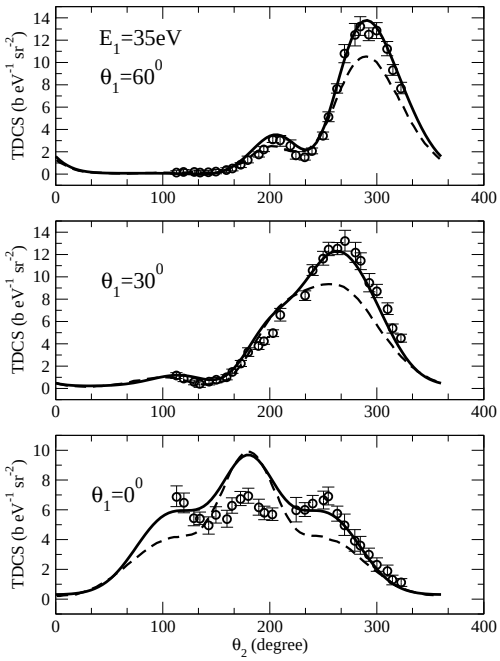

FIG. 11: TDCS for photon energy 40 eV above threshold, in the unequal energy sharing of $E_1 = 35$ eV and $E_2 = 5$ eV at various θ_1 of the 35 eV electron. Circles and dashed curve: experiment and CCC calculation of Ref. [49]. Thick solid curve: Present result.

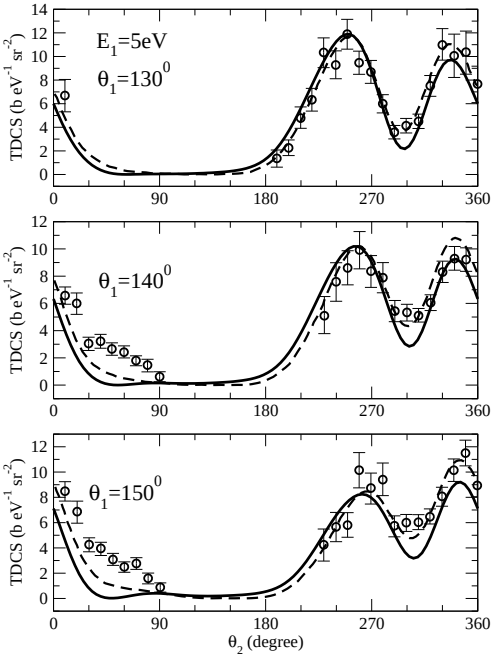

FIG. 12: TDCS for photon energy 40 eV above threshold, in the unequal energy sharing of $E_1 = 5$ eV and $E_2 = 35$ eV at various θ_1 of the 5 eV electron. Circles: experimet of Cvejanović *et al.* [50] Dashed curve: CCC calculation [51]. Thick solid curve: Present result.

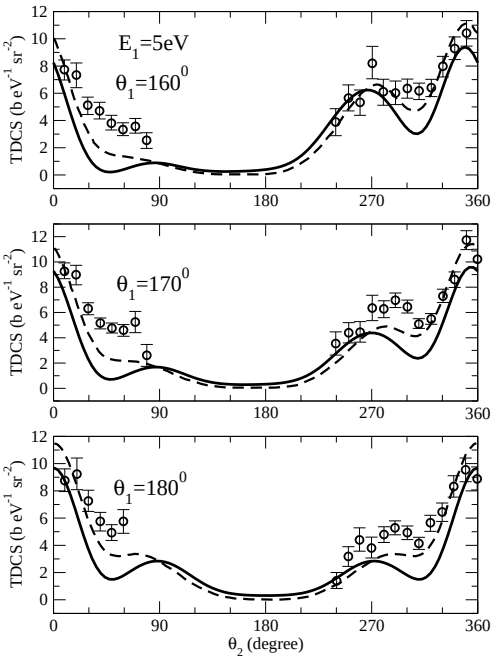

FIG. 13: TDCS for photon energy 40 eV above threshold, in the unequal energy sharing of $E_1 = 5$ eV and $E_2 = 35$ eV at various θ_1 of the 5 eV electron. Circles: experimet of Cvejanović *et al.* [50] Dashed curve: CCC calculation [51]. Thick solid curve: Present result.